

Expression Pattern of T-type Ca²⁺ Channels in Embryonic Chick Nodose Ganglion Neurons

Judith Pachuau, Miguel Martin-Caraballo

Department of Biology, University of Vermont, Burlington, Vermont 05405

Received 12 March 2007; revised 17 July 2007; accepted 19 July 2007

ABSTRACT: In this study we have characterized the functional expression of T-type Ca²⁺ channels in developing chick nodose neurons, a population of placode-derived sensory neurons innervating the heart and various visceral organs. Voltage-gated Ca²⁺ currents were measured using whole cell patch clamp recordings in neurons acutely isolated between embryonic day (E) 7 and E20, prior to hatching. E7 nodose neurons express relatively large high voltage-activated (HVA) Ca²⁺ currents. HVA current density progressively increases between E7 and E17. T-type Ca²⁺ currents were restricted to a few nodose neurons between E7 and E10 but were present in ~60% of nodose neurons by E17. T-type Ca²⁺ channels regulate the response of nodose neurons to injection of hyperpolarizing currents, but do not have any effect on the action potential waveform. Nickel ions blocked T-type Ca²⁺ currents in

a concentration-dependent manner with an IC₅₀ of 17 μM. The high sensitivity of T-type Ca²⁺ channels to nickel blockade combined with sequencing of a partial cDNA suggests that T-type Ca²⁺ currents are generated by α1H subunits in chick nodose neurons. Steady-state activation and inactivation kinetics were similar to those previously reported for other α1H channels in mammalian neurons. Semi-quantitative PCR analysis indicates that α1H mRNA was present in chick nodose neurons by E7, suggesting that the functional expression of T-type Ca²⁺ channels involves a posttranscriptional mechanism. These findings demonstrate a distinct pattern of T-type Ca²⁺ channel functional expression in placode-derived neurons when compared with CNS neurons. © 2007 Wiley Periodicals, Inc. *Develop Neurobiol* 67: 1901–1914, 2007

Keywords: development; calcium channel; expression

INTRODUCTION

Low voltage-activated (or T-type) Ca²⁺ channels are a particular group of voltage-gated Ca²⁺ channels that display low threshold activation, fast inactivation, and tiny conductance. Ca²⁺ influx through T-type Ca²⁺ channels regulates various developmental processes including neurite outgrowth and electrical differentiation (Holliday and Spitzer, 1990; Gu and

Spitzer, 1993; Chemin et al., 2002). Activation of T-type Ca²⁺ channels regulates the action potential waveform and repetitive firing pattern in developing spinal neurons (Umemiya and Berger, 1994; Martin-Caraballo and Greer, 2001). Thus, age-dependent changes in T-type Ca²⁺ channel expression can have a significant effect on the electrical properties of developing neurons. Previous studies have shown that functional expression of T-type Ca²⁺ channels is downregulated in CNS neurons during early differentiation (McCobb et al., 1989; Chambard et al., 1999; Schmid and Guenther, 1999; Martin-Caraballo and Greer, 2001). Whether this constitutes a general pattern of channel expression throughout the developing nervous system is unclear.

Understanding the molecular nature and biophysical properties of T-type Ca²⁺ channels in a particular neuronal population is critical for understanding their

Correspondence to: M. Martin-Caraballo (miguel.martin-caraballo@uvm.edu).

Contract grant sponsor: University of Vermont, and Vermont Genetics Network through grant number P20 RR16462 from the INBRE Program of the National Center for Research Resources (NCRR), a component of the National Institutes of Health (NIH).

© 2007 Wiley Periodicals, Inc.

Published online 14 September 2007 in Wiley InterScience (www.interscience.wiley.com).

DOI 10.1002/dneu.20563

functional role and regulation during neuronal development. In mammals, the pore-forming $\alpha 1$ subunit of T-type Ca^{2+} channels is encoded by three different genes: $\text{Ca}_v3.1$ (which encodes $\alpha 1G$ subunits), $\text{Ca}_v3.2$ ($\alpha 1H$), and $\text{Ca}_v3.3$ ($\alpha 1I$) (Cribbs et al., 1998; Perez-Reyes et al., 1998; McRory et al., 2001). Although Ca^{2+} currents generated by $\alpha 1G$, $\alpha 1H$, and $\alpha 1I$ subunits are activated by more negative membrane potentials and show very tiny conductance and fast inactivation, they differ in their biophysical and pharmacological properties including inactivation and deactivation kinetics and sensitivity to nickel ions (Perez-Reyes et al., 1998; Klockner et al., 1999; Lee et al., 1999; Chemin et al., 2002). Alternative splicing also contributes to the large diversity of functional properties of T-type Ca^{2+} channels in different populations of neurons (Mittman et al., 1999; Chemin et al., 2001; Murbartian et al., 2002).

Chick nodose ganglion neurons are a useful model to study various aspects of neuronal development but their electrophysiological differentiation has remained largely overlooked (Lindsay et al., 1985; Larmet et al., 1992; Forgie et al., 1999). Nodose neurons are sensory neurons that innervate the heart and other visceral organs in order to convey information to the CNS regarding elevation in blood pressure, heart and lung distension, and changes in blood oxygenation (reviewed by Zhuo et al., 1997). There is evidence that disruption of nodose innervation to the chick heart can result in abnormal cardiac function due to prolonged QT interval (Mulroy and Harrison, 1994; Harrison et al., 1995). Unlike autonomic or dorsal root ganglia neurons that originate from the neural crest, nodose cells are placode-derived. Nodose neurons in the chick are generated between embryonic day (E) 2 and E5 (D'Amico-Martel, 1982; Harrison et al., 1994). Around E5, nodose neurons begin to extend axons toward the heart and other visceral targets (Vogel and Davies, 1991). Failure to make appropriate connections with their peripheral and central targets results in the elimination of $\sim 50\%$ of the initial number of nodose neurons by E15 (Harrison et al., 1994). High voltage-activated (HVA) Ca^{2+} currents in nodose neurons are first detected at stage 23 (corresponding to E3 $\frac{1}{2}$ –E4) but not at stage 18 (\sim E2 $\frac{1}{2}$, Larmet et al., 1992). The normal pattern of HVA Ca^{2+} channel expression occurs *in vitro* independently of culture conditions, suggesting that epigenetic factors do not play a role in the regulation of HVA Ca^{2+} channel expression. Little is known regarding the developmental regulation of T-type Ca^{2+} channels in developing neurons including nodose neurons. In the present study we have characterized the functional expression of T-type Ca^{2+}

channels in chick nodose neurons between E7 and E20. Our present results indicate that during this period of neuronal differentiation, there is a significant increase in the functional expression of T-type Ca^{2+} channels. T-type Ca^{2+} currents in chick nodose neurons are generated by $\alpha 1H$ subunits with similar properties to those found in mammalian neurons.

METHODS

Dissociated Cell Cultures

Nodose ganglia were isolated from chick embryos at various developmental stages (E7, E10, E17, and E20). The ganglia were excised into a HEPES-based, Ca^{2+} - and Mg^{2+} -free solution, mildly trypsinized [0.05% trypsin for 12 min (E7); 15 min (E10); 18 min (E17); and 25 min (E20)], dissociated by trituration, and plated onto poly-D-lysine-coated glass coverslips. Basal culture medium consisted of Eagle's minimal essential medium (MEM, Bio-Whittaker, Walkersville, MA) supplemented with 10% heat-inactivated horse serum, 2 mM glutamine, 50 U/mL penicillin, and 50 $\mu\text{g}/\text{mL}$ streptomycin. Cell cultures were maintained in a 5% CO_2 incubator at 37°C for several hours. To study the expression of ionic currents in acutely dissociated neurons, recordings were made 3–4 h after nodose ganglia dissociation. Immediately after isolation, nodose neurons have a round morphology (Harrison et al., 1994) but after a few hours in culture, nodose neurons begin to grow one or two short neurites from the cell body.

Electrophysiology

Neurons from dissociated nodose ganglia were visualized using an Olympus X71 inverted microscope equipped with Hoffman optics. Recordings were performed at room temperature (22–24°C). Recording electrodes were made from thin wall borosilicate glass (3–4 M Ω) and filled with a solution consisting of 120 mM CsCl, 2 mM MgCl_2 , 10 mM HEPES, 10 mM EGTA, 1 mM ATP, and 0.1 mM GTP (pH 7.4 with CsOH). Normal external saline for measurements of Ca^{2+} currents contained 145 mM tetraethylammonium chloride (TEACl), 10 mM CaCl_2 , and 10 mM HEPES (pH 7.4 with CsOH). In the Ca^{2+} -free solution, Ca^{2+} ions were replaced by an equimolar concentration of Mg^{2+} , a divalent cation that does not permeate voltage-gated Ca^{2+} channels. To measure Ca^{2+} currents, a 200 ms-depolarizing step to various potentials was applied from either a holding potential of -100 or -60 mV in normal external saline and following a 3 min incubation in Ca^{2+} -free external saline. Net current amplitude was obtained by digital subtraction (control: Ca^{2+} -free). Ca^{2+} channel antagonists were applied by a gravity-fed perfusion system. Voltage commands and data acquisition and analysis were performed with a MULTICLAMP 700A amplifier and PCLAMP software (Axon Instruments, Foster City, CA). The MultiClamp 700B Commander was used to compensate for pipette offset, whole cell capacitance, and series resistance (usually <10 M Ω , up

to 80% compensation was used when necessary). Inadequate space clamp was minimal in acutely isolated nodose neurons because of their round shape devoid of dendritic processes. A minority of cultured neurons was discarded from further analysis because of insufficient space clamp as evidenced by the lack of T-type Ca^{2+} channel inactivation. For quantitative analyses, we normalized for cell size by dividing current amplitudes by cell capacitance, determined by integration of the current transient evoked by a 10-mV voltage step from a holding potential of -60 mV (Martin-Caraballo and Dryer, 2002).

The inactivation time constant was obtained by fitting the decay portion of the transient currents with one exponential function in the form $I(t) = A \exp(-t/\tau)$, where A is peak current and τ is the time constant. Steady-state activation curves were obtained from current–voltage (I/V) relationships using the equation $G = I/(V - V_r)$ where I is the current at a given voltage, V is the voltage command, and V_r is the reversal potential of calcium currents obtained by extrapolating the ascending portion of the current–voltage curve. Conductance values were normalized to the maximum conductance at -20 mV and plotted as a function of voltage before being fitted with a Boltzman equation in the form $G/G_{max} = (1 + \exp(V_{1/2} - V)k)^{-1}$ where G is conductance at membrane voltage V , G_{max} is maximal conductance at -20 mV, $V_{1/2}$ is the half-activation voltage, and k is the slope factor. Steady-state inactivation curves were fitted with a Boltzman equation using normalized current values $I/I_{max} = (1 + \exp(V_{1/2} - V)k)^{-1}$ where I is current at membrane voltage V , I_{max} is maximal current with the -100 mV conditioning prepulse, $V_{1/2}$ and k have the same meaning as above. The nickel dose-response curves were fitted with a Hill equation in the form $I(x) = [1 + (IC_{50}/x)^n]^{-1}$, where IC_{50} is the drug concentration at half maximal block, and n is the Hill coefficient.

Membrane voltage responses to injection of hyperpolarizing or depolarizing currents were recorded in current clamp mode. Recordings were performed using the following external solution: 145 mM NaCl, 5.4 mM KCl, 0.8 mM $MgCl_2$, 5.4 mM $CaCl_2$, 5 mM glucose, 13 mM HEPES (pH 7.4 with NaOH). The composition of the pipette solution was 120 mM KCl, 2 mM $MgCl_2$, 10 mM HEPES, 10 mM EGTA (pH 7.4 with KOH). Action potentials were generated by injection of 2 ms-long depolarizing pulses. Action potential duration was recorded at half maximal amplitude as previously reported (Martin-Caraballo and Greer, 2001). The amplitude of the hyperpolarizing potential was measured at the point of maximal voltage deflection from holding potential.

RNA Isolation, Amplification, Cloning, and Sequencing of T-type Ca^{2+} Channel Partial cDNA

Total RNA was extracted from homogenized nodose ganglia by TRIzol reagent according to the manufacturer's instructions (Invitrogen, CA). Total RNA was used as a template to synthesize single-stranded cDNA using Superscript III reverse transcriptase and 12–18 oligo-dT primers

(Invitrogen, CA). RT mix containing 1 μ g RNA was incubated for 60 min at $55^\circ C$. Amplification of primer-specific cDNA was performed by polymerase chain reaction using Taq DNA polymerase (Invitrogen, CA). Specific oligonucleotide primers were designed against conserved regions of all rat subunits ($\alpha 1G$, $\alpha 1H$, $\alpha 1I$) spanning a region between the III-S2 and the III-S6 domains consisting of: (forward primer) 5'-CAT ATT TCT CAA CTG CAT TAC AAT AGC ACT GG-3' and 5'-TCC ACC ACC ACC CCC ACG AAC ATG TTG AGC-3' (reverse). cDNA was amplified according to the following protocol: $95^\circ C$ for 10 min, $57^\circ C$ for 1 min (50 cycles), and $60^\circ C$ for 1 min. PCR products were separated on 1.5% low melting point agarose gels. Bands were excised and submitted for sequencing at the Vermont Cancer Center DNA facility on an Applied Biosystems DNA sequencer.

Semi-Quantitative RT-PCR Analysis of T-type Ca^{2+} Channel cDNA

RNA isolation and cDNA synthesis was performed as described above. The cDNA was used as a template for the RT-PCR reaction using Taq DNA polymerase (Invitrogen). Trial experiments were performed in order to determine the optimal range of cDNA concentrations and PCR cycles required for transcript detection within the linear phase of amplification for each set of primers. The housekeeping gene glyceraldehyde-3-phosphate dehydrogenase (GAPDH) was amplified with 20 cycles to normalize for the cDNA content of each sample, whereas T-type Ca^{2+} channel cDNA was amplified with 45 cycles using the set of primers described earlier. Amplicons were separated on 1.5% low melting point agarose gels and stained with ethidium bromide. Pictures of the gels were obtained with a digital imaging system (ChemIDoc RXS System, Bio-Rad). Band intensities were obtained by integrating the area of each band (Quantity One software, Bio-Rad). For each age, relative gene expression was determined by the ratio of band intensities (target gene divided by housekeeping gene) in three different samples.

Data Analysis

Averaged data values are presented as mean \pm SEM. Where indicated, statistical analyses consisted of Student's unpaired t -test when single comparisons were made, or one-way ANOVA followed by *post hoc* analysis using Tukey's honest significant difference test for unequal n for comparisons between multiple age groups (STATISTICA software, Tulsa, OK). Throughout, $p \leq 0.05$ was regarded as significant. In every experiment, data were collected from a minimum of two platings (i.e. from multiple cultures).

RESULTS

To characterize the expression of voltage-gated Ca^{2+} channels in developing chick nodose neurons, Ca^{2+}

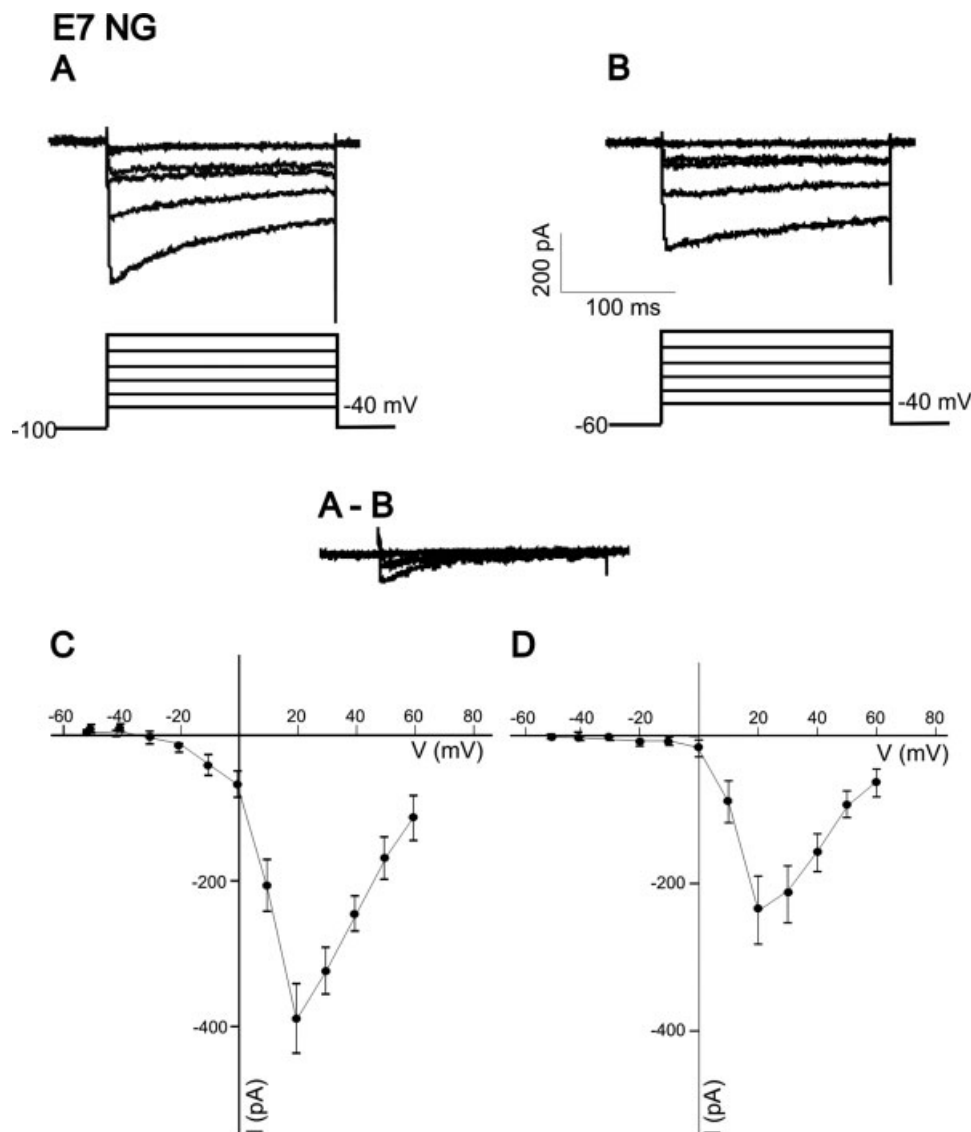


Figure 1 Ca^{2+} currents in an E7 nodose neuron. (A) Typical current traces in E7 nodose neurons obtained from a holding potential of -100 mV. In this and subsequent figures, the voltage step protocol is shown below the current trace. (B) Current traces in the same neuron obtained from a holding potential of -60 mV (corresponding voltage step protocol shown at the bottom) Notice that most of the inactivating component observed in A is eliminated when neurons are stepped from a more depolarized holding potential. (A-B) Digital subtraction of A and B traces shows the inactivating component. (C,D) Current-voltage (I - V) relationship for the peak currents generated from a holding potential of -100 or -60 mV in E7 nodose neurons ($n = 12$).

currents were isolated by substitution of Na^+ ions with external tetraethylammonium and by blocking outward K^+ currents with Cs^+ ions in the pipette solution. Macroscopic Ca^{2+} currents were evoked by a series of 200 ms long depolarizing steps from a holding potential of -100 or -60 mV to differentiate between T-type and HVA currents, respectively. By E7, nodose neurons expressed relatively large Ca^{2+} currents that were blocked by perfusion with a Ca^{2+} -

free extracellular solution (see Methods). A typical set of current traces for an E7 and E17 nodose neuron is represented in Figures 1 and 2, respectively. Voltage steps to more positive membrane potentials from a -100 mV holding potential revealed large inward currents with both inactivating and noninactivating components at all ages tested [Figs. 1(A) and 2(A)]. The inactivating component was significantly reduced when neurons were depolarized from a hold-

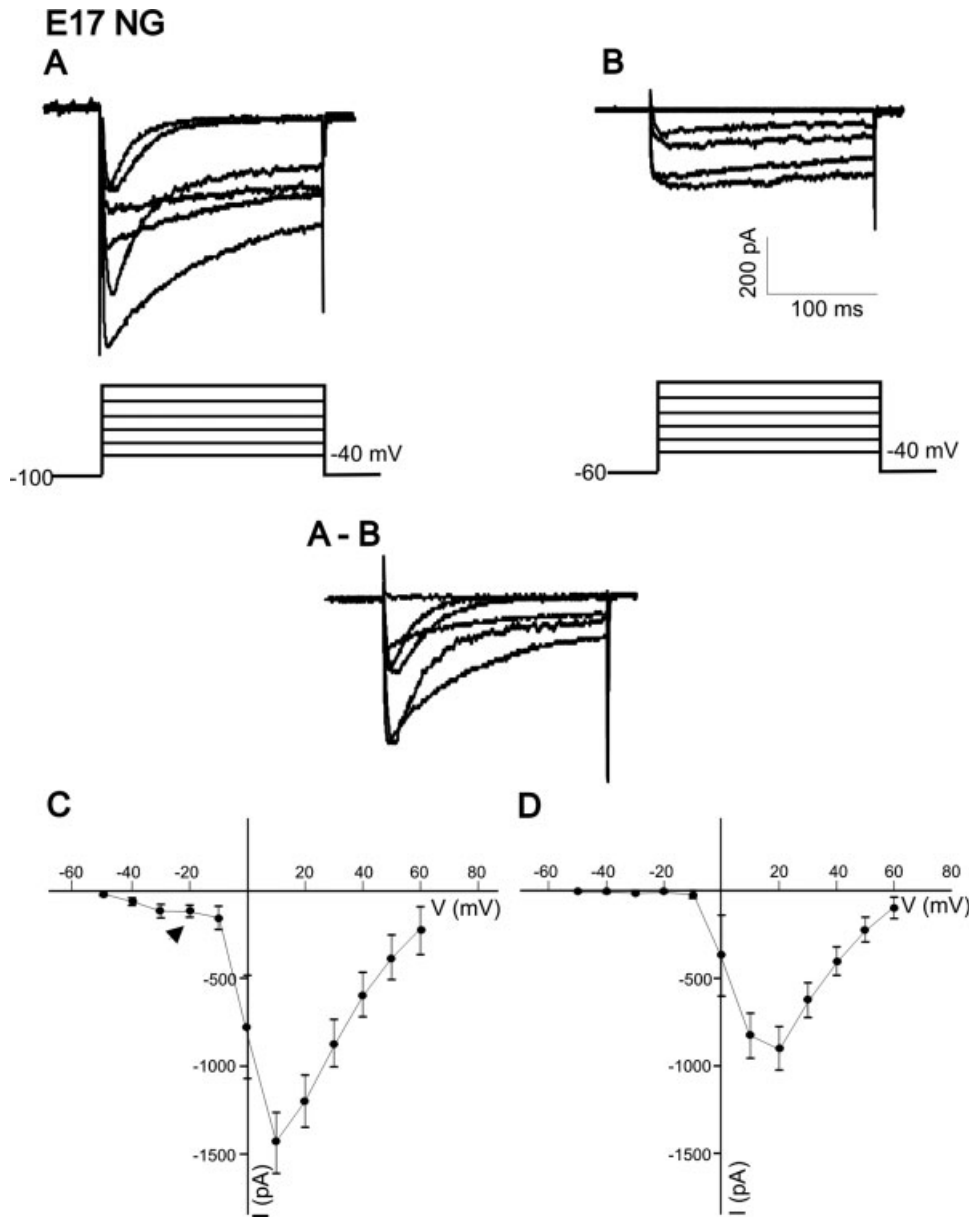


Figure 2 Ca^{2+} currents in an E17 nodose neuron. (A) Typical current traces in E17 nodose neurons obtained from a holding potential of -100 mV. (B) Current traces in the same neuron obtained from a holding potential of -60 mV. (A-B) Digital subtraction of A and B traces shows the remaining T-type component. (C,D) Current-voltage (I - V) relationship for the peak currents generated from a holding potential of -100 or -60 mV in E17 nodose neurons ($n = 11$). At E17, the majority of nodose neurons have a low threshold, transient component that appears as a shoulder in the I - V relationship (see arrow in C).

ing potential of -60 mV when compared to -100 mV [Figs. 1(B) and 2(B)]. At all ages tested, maximum current amplitudes were generated by voltage steps between $+10$ and $+20$ mV. The current-voltage relationship for E7 nodose neurons is shown in Figure 1(C,D). In a majority of E17 and E20 neurons, depolarizations from a holding potential of -100 mV

also revealed a transient component (or T-type current) that activated at relatively more negative potentials. The transient component was activated at potentials between -50 and -40 mV and reached a peak at -20 mV [Fig. 2(A,B)]. T-type currents activated relatively slowly (time to peak for E17 neurons, 11 ± 0.9 ms, $n = 21$; for E20, 11.5 ± 0.7 , $n = 26$) and

had a fast inactivation as indicated by its decay to near 0 in less than 100 ms during a sustained depolarization (decay time constant for E17, 33.5 ± 4.4 ms, $n = 20$; for E20, 34.2 ± 3.7 , $n = 26$). The presence of this early transient component was evident from the shoulder in the IV plots at more negative potentials [Fig. 2(C), arrow]. T-type Ca^{2+} currents were present in a majority of E17–E20 nodose neurons, but found in only a few E7 and E10 neurons (see below).

The biophysical properties of T-type Ca^{2+} currents were further characterized in E20 nodose neurons. To determine the steady-state activation properties of T-type Ca^{2+} channels, the relative conductance was plotted against depolarizing voltage steps and fitted by a Boltzmann equation [Fig. 3(B)]. Fitting of the activation curve yielded $V_{1/2} = -37.0 \pm 1.0$ mV (step potential resulting in half maximal activation of normalized conductance) and $k = 3.6 \pm 1$ mV [steepness of the curve, Fig. 3(B)]. The steady-state inactivation of T-type Ca^{2+} channels in E20 nodose neurons was studied using a 200 ms-test pulse to -20 mV preceded by a series of 5s-conditioning prepulses between -100 and -30 mV [Fig. 3(A)]. The relative amplitude of the peak current was plotted as a function of the prepulse potential and fitted by a Boltzmann function [Fig. 3(B)]. Inactivation was completely removed at potentials more negative than -80 mV, whereas at potentials more positive than -50 mV, inactivation became complete. The mean half-inactivation potential ($V_{1/2}$) and the slope factor were -66.9 ± 1.3 mV and 4.3 ± 0.3 mV ($n = 12$), respectively. There was very little overlap of the activation and inactivation curves under our recording conditions. To study the rate of T-type Ca^{2+} channel closing or deactivation, E20 nodose neurons were stepped to -20 mV from a holding potential of -100 mV for 10 ms followed by repolarization to potentials from -40 to -100 mV (Fig. 4). Representative deactivating tail currents are illustrated in Figure 4(A). T-type Ca^{2+} current deactivation was best fitted with a single exponential function. The voltage dependence of the deactivation constant as a function of voltage is represented in Figure 4(B). The deactivation time constant (τ_d) was nearly flat between -100 and -70 mV and increased significantly at voltages above -60 mV [$\tau_d = 9.5 \pm 1.5$ ms at -100 mV; $\tau_d = 29.0 \pm 2.3$ ms at -40 mV, Fig. 4(B)].

It has been reported that low nickel concentrations can block T-type Ca^{2+} currents (Barish, 1991). To investigate the effect of Ni^{2+} on T-type currents, nodose neurons were depolarized by a step potential to -20 mV (from a holding potential of -100 mV). Ni^{2+} application ($100 \mu\text{M}$) caused a significant inhibition of T-type currents in nodose neurons [Fig. 5(A,C)].

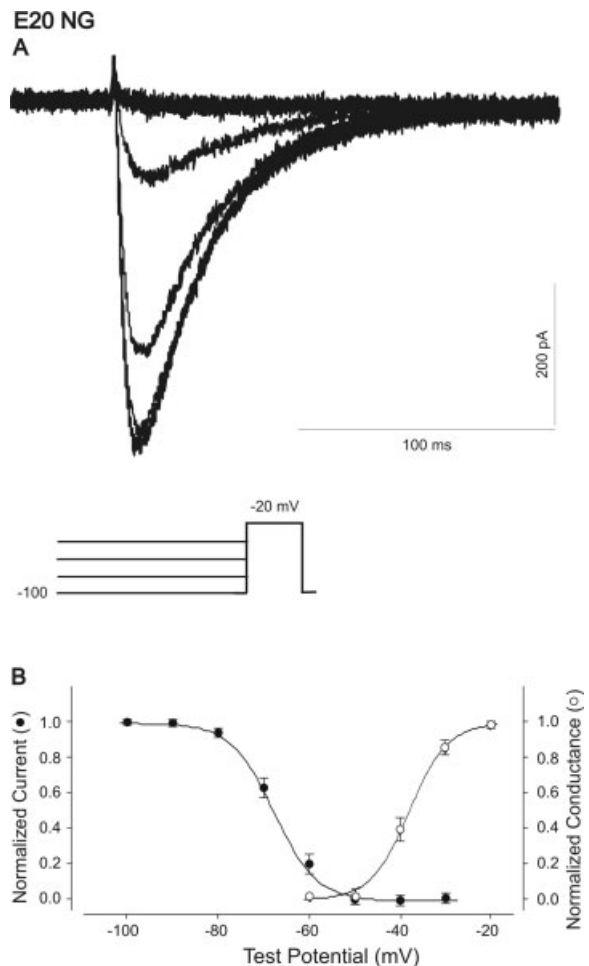


Figure 3 Steady-state activation and inactivation of T-type Ca^{2+} channels in E20 chick nodose neurons. (A) Typical sample traces showing steady-state inactivation of T-type Ca^{2+} channels in an E20 neuron. Membrane potential was held at voltages ranging from -100 to -30 mV for 5 s before applying a 200 ms depolarizing step to -20 mV (lower trace in A represents the voltage protocol used). (B) Voltage dependence of steady-state activation (open circles) and inactivation (filled circles) curves. The solid line represents the best fit obtained with a Boltzmann equation for steady-state activation and inactivation values ($n = 12$).

At a test potential of $+20$ mV, Ni^{2+} ions did not have a significant effect on the amplitude of the HVA component [Fig. 5(B)]. Figure 5(C) shows the relationship between T-type currents as a function of Ni^{2+} concentration. These values were fitted with the equation $I(x) = [1 + (\text{IC}_{50})/x^n]^{-1}$ in order to assess the drug concentration resulting in half maximal block (IC_{50}) and the Hill coefficient (n). Fitting of the averaged dose response points from five neurons indicates an IC_{50} value equal to $17 \mu\text{M}$, whereas the Hill coefficient was 0.8, suggesting that T-type Ca^{2+} channels

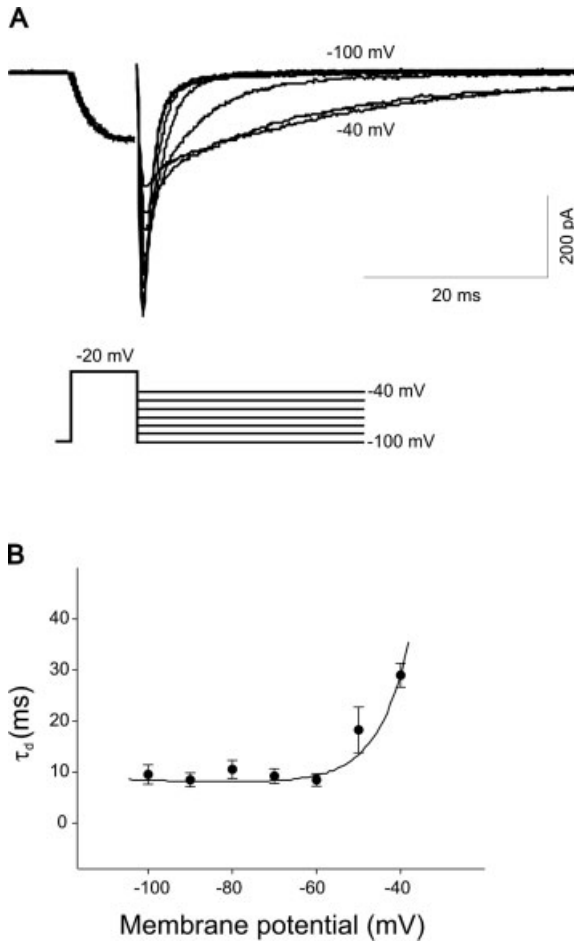


Figure 4 Voltage dependence of deactivation of T-type Ca^{2+} channels in E20 nodose neurons. (A) Tail currents generated by a test pulse to -20 mV from a holding potential of -100 mV, were followed by deactivation potentials between -40 and -100 mV by sequential depolarizing steps of 10 mV. (B) Deactivation time constants were obtained by fitting tail currents with a single exponential and were plotted as a function of the deactivation potential ($n = 10$).

in E20 nodose neurons are very sensitive to Ni^{2+} block.

Developmental Changes in T-type and HVA Ca^{2+} Channel Expression

To study the developmental expression of Ca^{2+} currents, nodose neurons were acutely isolated at various stages of development and the functional expression of Ca^{2+} currents was determined by whole cell recordings. To compensate for changes in cell size that occur throughout these developmental stages, whole-cell currents were normalized to cell capacitance (see Methods). Between E7 and E20, cell

capacitance increased steadily from ~ 15 to 25 pF [Fig. 6(A)]. Although not directly assessed here, the increased cell capacitance is most likely due to increase in cell diameter (Harrison et al., 1994). Since HVA Ca^{2+} currents are an early feature of developing nodose neurons (Larmet et al., 1992), we first assessed developmental changes in HVA Ca^{2+} current densities. As represented in Figure 6(B), peak current densities for HVA currents recorded at $+20$

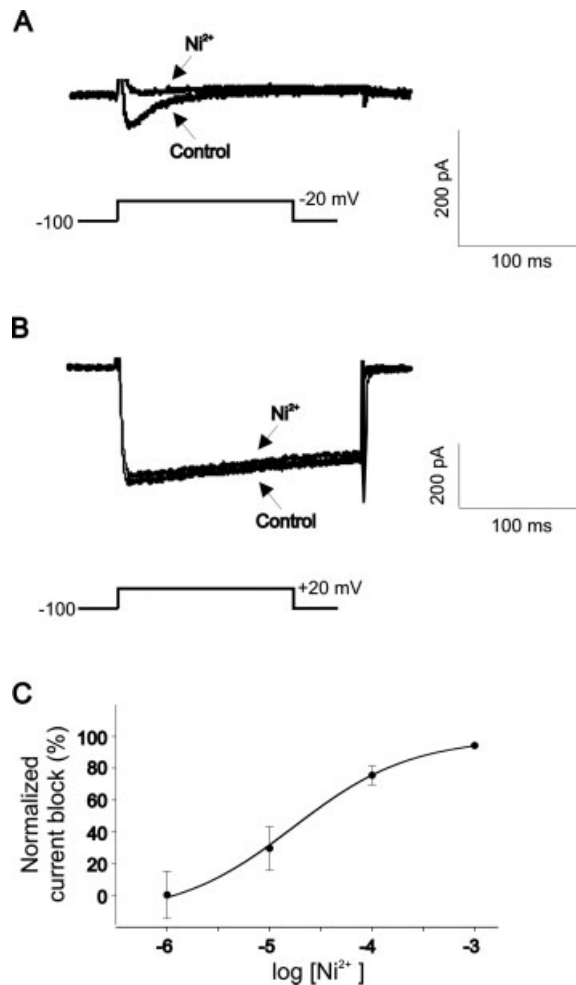


Figure 5 Effect of Ni^{2+} ions on Ca^{2+} currents in nodose neurons. (A) The T-type Ca^{2+} current generated by a voltage step to -20 mV from a holding potential of -100 mV was eliminated following incubation with $100 \mu\text{M}$ Ni^{2+} . (B) The HVA Ca^{2+} component generated by a voltage step to $+20$ mV was less sensitive to Ni^{2+} as indicated by a $<10\%$ -inhibition of control current. (C) Dose response of T-type Ca^{2+} currents to increasing concentrations of Ni^{2+} . Normalized current block from five neurons (expressed as a percentage of control currents before Ni^{2+} application) was plotted as a function of Ni^{2+} concentration. The solid line represents the best fit of averaged points with the Hill equation (see Methods).

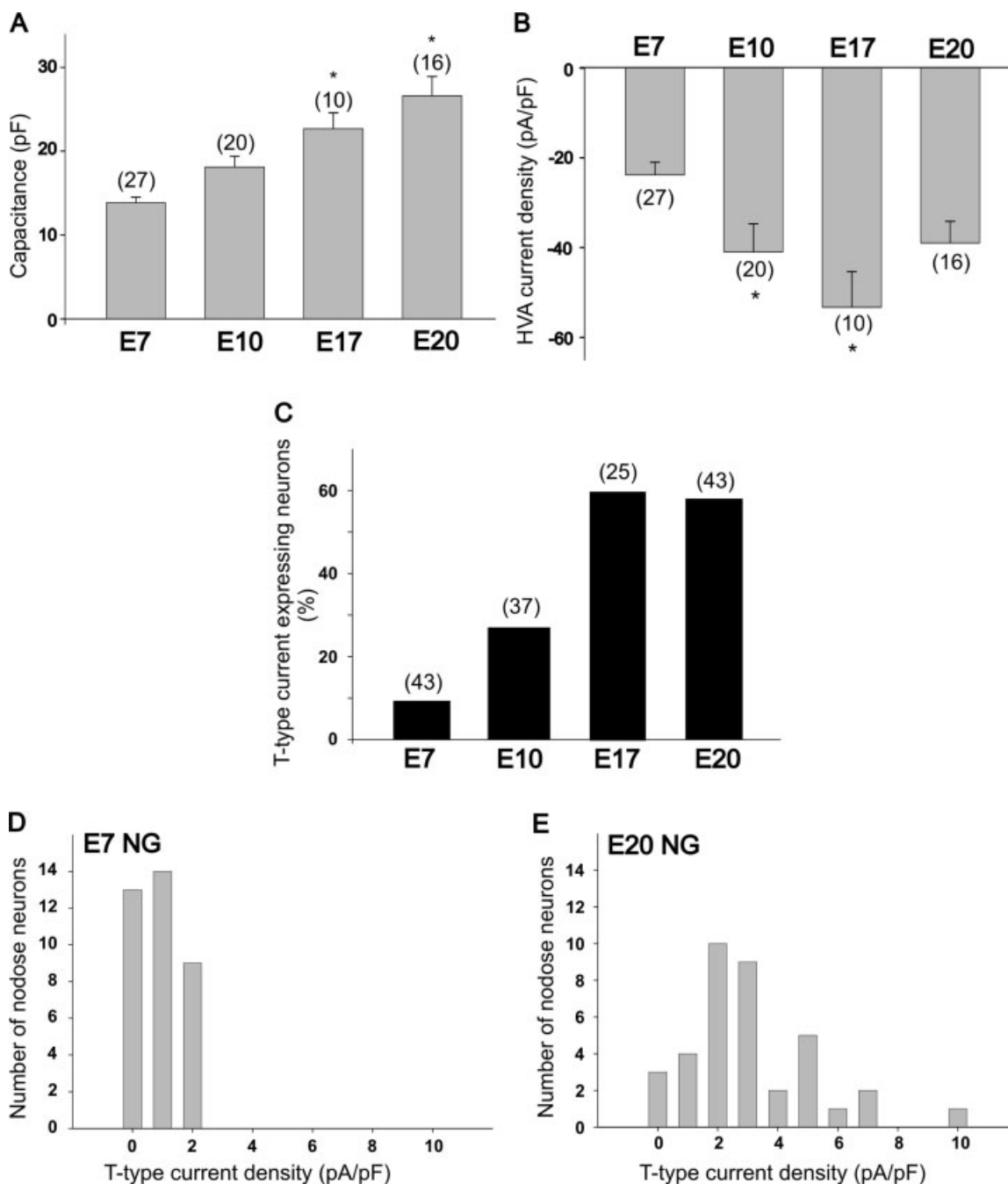


Figure 6 Developmental changes in the expression of HVA and T-type Ca^{2+} currents in acutely isolated nodose neurons. (A) Mean cell capacitance between E7 and E20 in acutely isolated nodose neurons. Notice significant increase in cell size during normal development of nodose neurons. (B) Peak HVA current density generated by a voltage step to +20 mV from a holding potential of -100 mV. (C) Population plot of T-type expressing neurons at different developmental stages. (D,E) Histograms of T-type Ca^{2+} current densities in E7 (D), and E20 (E) nodose neurons. Ca^{2+} currents were generated by 200 ms depolarizing pulses to -20 from a holding potential of -100 mV. Note the rightward shift in the number of nodose neurons expressing high current densities between E7 and E20. In A and B, results are mean \pm SEM and (*) denotes $p \leq 0.05$ from E7 as determined by one-way ANOVA followed by Tukey's honest significant difference test for unequal n . The number of cells recorded under each experimental condition is given above each bar.

mV increased nearly threefold between E7 and E17. Expression of T-type Ca^{2+} currents was also developmentally regulated: between E7 and E10 a minority of neurons expressed the transient component [Fig. 6(C)]. However, by E17, ~60% of nodose neurons expressed T-type Ca^{2+} currents. T-type Ca^{2+} current expression was significantly high in E20 neurons as well. Age-dependent changes in T-type Ca^{2+} current expression resulted in a rightward shift in the distribution of current densities constructed for E7 and E20 nodose neurons [Fig. 6(D,E)].

Role of T-type Ca^{2+} Channels in Regulating the Action Potential Waveform and Hyperpolarizing Membrane Responses

Membrane responses to hyperpolarizing or depolarizing current injections were studied to assess the functional role of T-type Ca^{2+} channels in E17–E20 nodose neurons. Injection of 300 ms long hyperpolarizing current pulses generated a rebound depolarization [Fig. 7(A), arrow]. At E20, ~61% of recorded neurons exhibited rebound depolarizations (11 out of 18 nodose neurons recorded). Increasing the strength of the hyperpolarizing current can ultimately result in the generation of an action potential when the rebound depolarizing potential reaches threshold. Incubation with $100 \mu\text{M}$ Ni^{2+} ions inhibited the generation of rebound depolarizations in all neurons tested ($n = 6$, 100% inhibition), indicating that T-type Ca^{2+} channels are responsible for this membrane response [Fig. 7(A), right traces]. The inhibitory effect of Ni^{2+} on the rebound depolarization was reversible (not shown). Injection of brief depolarizing pulses resulted in the generation of action potentials [Fig. 7(B)]. At E20, nodose neurons exhibited brief overshooting spikes (action potential amplitude = 99 ± 2 mV, duration = 2.6 ± 0.4 ms, $n = 15$) followed by a long lasting hyperpolarizing potential [50–200 ms duration, empty arrow in Fig. 7(B)]. Incubation of nodose neurons with $100 \mu\text{M}$ Ni^{2+} did not alter the action potential waveform [Fig. 7(B)]. Thus, Ni^{2+} application had no effect on action potential amplitude (100 ± 3 vs. 102 ± 6 mV, $n = 6$, $p > 0.5$), duration (2.0 ± 0.3 vs. 1.8 ± 0.3 ms, $n = 6$, $p > 0.5$), or hyperpolarizing potential amplitude (10 ± 3 vs. 11 ± 3 mV, $n = 6$, $p > 0.5$). These results suggest that the functional expression of T-type Ca^{2+} channels regulates the response of nodose neurons to inhibitory inputs but they have little effect on shaping the action potential waveform.

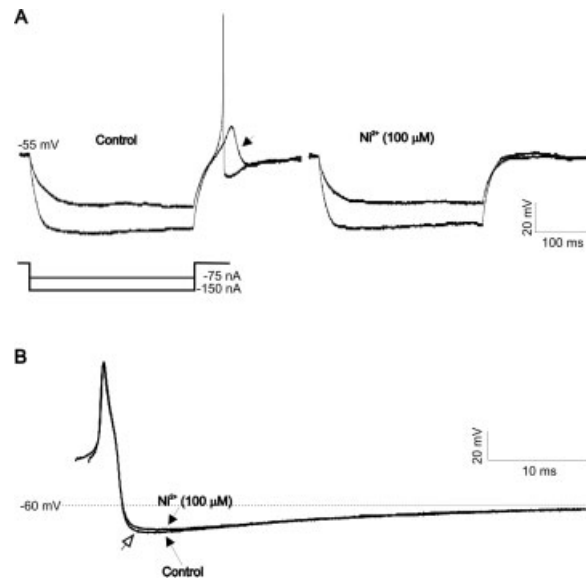


Figure 7 Effect of blocking T-type Ca^{2+} channels on the action potential waveform and rebound depolarization in E20 nodose neurons. (A) Membrane responses to injection of hyperpolarizing currents in an E20 nodose neuron. Notice injection of hyperpolarizing currents results in a rebound excitation (filled arrow) that can ultimately trigger an action potential. Both the rebound depolarization and action potential generation can be blocked with $100 \mu\text{M}$ Ni^{2+} . Rebound depolarizations were generated by injection of hyperpolarizing currents of increasing amplitude (lower trace). (B) Ni^{2+} ions have very little effect on the shape of the action potential waveform. Spikes were followed by a medium duration after hyperpolarizing potential (empty arrow). Action potentials were generated by brief injection of depolarizing currents (2 ms, 1.2 nA). For clarity, the stimulation artifact has been removed from the trace.

Cloning and Sequencing of a T-type Ca^{2+} Channel Partial cDNA From E20 Nodose Neurons

T-type Ca^{2+} currents generated by $\alpha 1\text{G}$, $\alpha 1\text{H}$, and $\alpha 1\text{I}$ subunits can display different biophysical and pharmacological properties (Perez Reyes et al., 1998; Klockner et al., 1999; Lee et al., 1999). To identify the $\alpha 1$ subunit that underlies T-type Ca^{2+} currents in chick nodose neurons, we designed a pair of PCR primers directed against conserved regions of all rat subunits ($\alpha 1\text{G}$, $\alpha 1\text{H}$, $\alpha 1\text{I}$) spanning a region between the III-S2 and the III-S6 transmembrane domains. PCR analysis yielded one amplification product of ~700 bp from total RNA extracted from E20 chick nodose neurons [Fig. 8(A), lane 2]. No products were amplified in control reactions lacking reverse transcriptase [Fig. 8(A), lane 3]. We should also point out that during our optimization process using different cycles

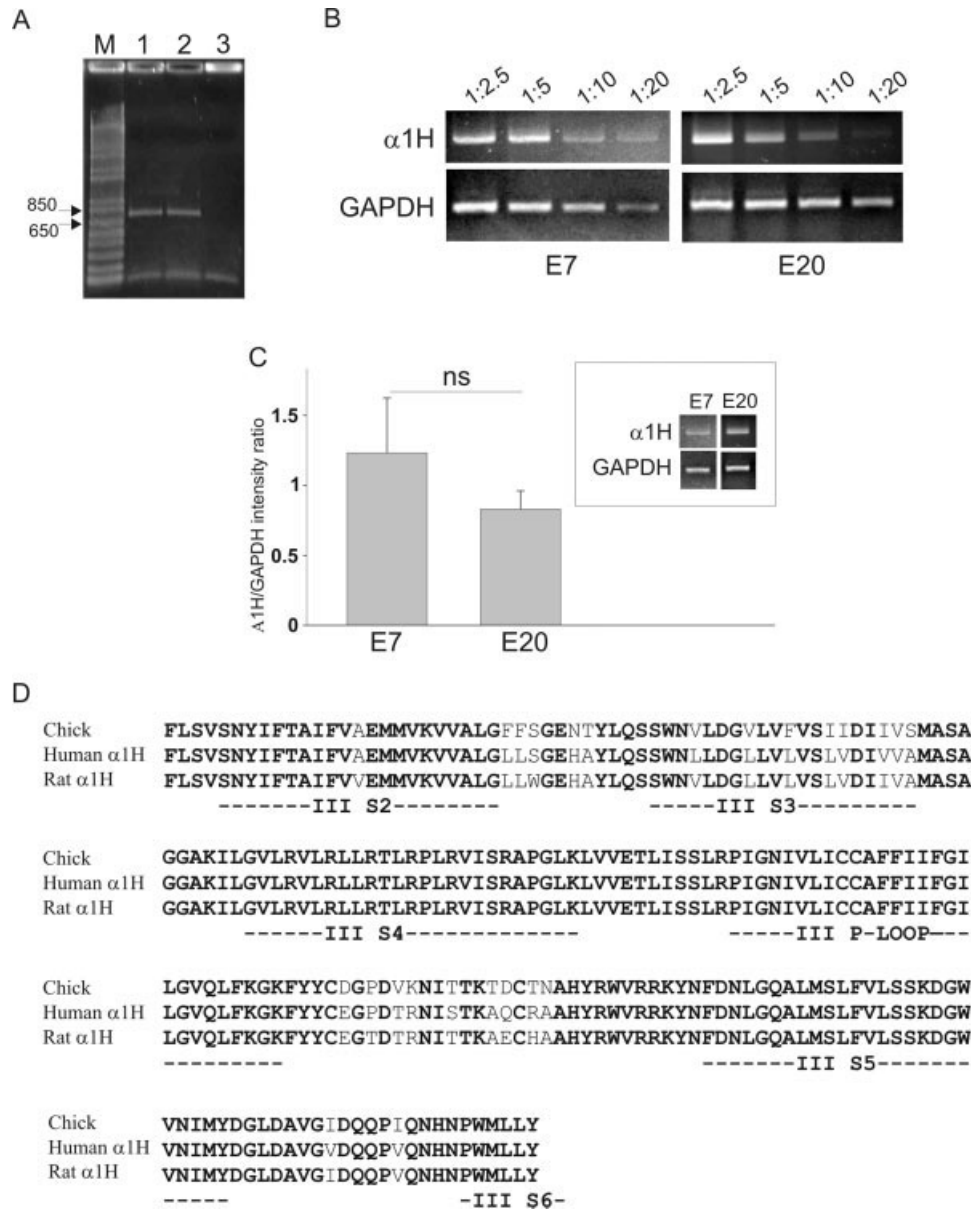


Figure 8 Molecular identification of α 1 subunit transcripts in chick nodose neurons. (A) RT-PCR detection of α 1 subunit transcripts in chick E7 (lane 1) and E20 (lane 2) nodose neurons. No products were obtained when the enzyme reverse transcriptase was omitted from the PCR reaction (lane 3). PCR products were amplified from cDNA obtained from total RNA of nodose ganglia. M represents the marker. Notice that RT-PCR analysis of nodose ganglia reveals a single band between 650 and 850 bp. (B) Amount of α 1H and GAPDH transcripts obtained by serial dilutions (1:2.5, 1:5, 1:10, and 1:20) of cDNA samples from E7 and E20 nodose ganglia. (C) Semi-quantitative PCR analysis of α 1H transcripts in E7 and E20 nodose ganglia. Relative expression of α 1H transcripts was normalized to the housekeeping gene GAPDH. Inset: examples of α 1H and GAPDH transcripts in E7 and E20 nodose ganglia. Results are mean \pm SEM ($n = 3$), “ns” denotes no significant differences as determined by Student’s unpaired *t*-test. (C) Alignment of the amino acid sequences of the deduced chick partial clone and rat and human α 1H subunits (GenBank accession numbers NM_153814 and AF051946, respectively). Conserved amino acids across all three species are represented in bold letters. The membrane-spanning segments (S2–S6) as well as the pore loop (P-loop) are represented with a discontinuous line below the sequence alignment (from McRory et al., 2001).

and annealing temperatures, we never saw more than one band (not shown). This PCR product was purified in low melting point agarose gel and sequenced. Sequence analysis of this PCR product generated a 647 bp partial cDNA that was blasted against a chick genome database (<http://www.ensembl.org>). BLAST analysis of our partial cDNA revealed that it is localized to chromosome 14 and is matched to a T-type Ca^{2+} channel homologous to the human gene coding for the $\alpha 1H$ subunit (Ensemble gene ID ENS-GALG0000005215). The amino acid sequence of our partial clone was determined using the program TRANSLATE on the ExPASy proteomics server (<http://www.expasy.org>). The deduced protein sequence of our partial clone is represented in Figure 8(D). The chick $\alpha 1H$ partial sequence was found to share an 89% similarity compared to the human and rat $\alpha 1H$ sequences. Most of the conserved amino acids are found in the membrane spanning and the pore-forming regions [Fig. 8(D)]. Homology with other $\alpha 1$ subunits was somewhat lower, including an 83% similarity to rat and human $\alpha 1I$ isoforms and 80% similarity to $\alpha 1G$ subunits. Interestingly, a similar PCR product was also present in E7 chick nodose ganglia although at this age there were very few functional T-type Ca^{2+} channels [Fig. 8(A), lane 1]). Age-dependent changes in $\alpha 1H$ subunit transcripts were determined by semi-quantitative RT-PCR using the housekeeping gene GAPDH as a normalizer [Fig. 8(B,C)]. Initially, we established that the yield of the RT-PCR reaction (assessed by the band intensity of $\alpha 1H$ and GAPDH transcripts) was a linear function of starting material [Fig. 8(B)]. Age-dependent changes in $\alpha 1H$ expression were quantified as band intensity ratios of $\alpha 1H$ and GAPDH transcripts. There was no significant difference in the $\alpha 1H$ /GAPDH transcript ratio between E7 and E20 nodose ganglia [Fig. 8(C)]. These results suggest that the functional expression of T-type Ca^{2+} channels in chick nodose neurons may be regulated by a posttranscriptional mechanism.

DISCUSSION

In this study we have characterized the expression of voltage-gated Ca^{2+} channels in embryonic chick nodose neurons using whole-cell recordings. Our current results indicate that HVA Ca^{2+} currents are found throughout all stages of embryonic development, whereas T-type Ca^{2+} channels show an incremental pattern of functional expression. On the basis of their sensitivity to nickel ions and sequencing analysis, we conclude that T-type Ca^{2+} currents are mediated by $\alpha 1H$ subunits in chick nodose neurons.

Expression of HVA Ca^{2+} Currents in Nodose Neurons

Nodose neurons express relatively large HVA Ca^{2+} currents as early on as E7. On the contrary, T-type Ca^{2+} currents are only found in less than 10% of all recorded neurons at this developmental stage, indicating that in differentiating nodose neurons HVA Ca^{2+} channels are expressed earlier than T-type channels. This finding is consistent with a previous report by Larnet et al. (1992), who were able to record HVA but not T-type Ca^{2+} channel expression at stage 23 (corresponding to E3½–E4). However, during neuronal differentiation of DRG neurons the opposite pattern of channel expression occurs (Gottmann et al., 1988), suggesting a significant variability in Ca^{2+} channel expression between different neuronal populations. Between E7 and E17, HVA current density progressively increases; however, a small reduction in HVA current density was noted in E20 nodose neurons. This age-dependent increase in HVA current density is similar to that described in other species and neuronal populations (McCobb et al., 1989; Desmadryl et al., 1998; Martin-Caraballo and Greer, 2001). HVA Ca^{2+} currents are evoked by Ca^{2+} influx through at least four distinct Ca^{2+} channels that are broadly divided into L-, N-, P-, and R-type Ca^{2+} channels (Fox et al., 1987; reviewed by Catterall, 1998). Ca^{2+} influx through HVA Ca^{2+} channels plays an important role in various cellular processes including neurotransmitter release, and regulation of electrical excitability and gene expression (Umehiya and Berger, 1994; Iwasaki et al., 2000; Martin-Caraballo and Greer, 2001). Ca^{2+} entry via HVA Ca^{2+} channels has also been implicated in the phenotypic differentiation of developing nodose neurons. For example, L-type Ca^{2+} channel activation mediates the activity-dependent induction of tyrosine hydroxylase in a subset of rat nodose neurons (Brosenitsch et al., 1998).

Expression of T-type Ca^{2+} Currents in Nodose Neurons

Three genes ($Ca_v3.1$, $Ca_v3.2$, and $Ca_v3.3$) encode the main pore-forming subunit of T-type Ca^{2+} channels in mammalian neurons ($\alpha 1G$, $\alpha 1H$, and $\alpha 1I$, respectively). Expression of individual subunits can generate functional channels with some striking differences. For example, transient Ca^{2+} currents generated by the expression of $\alpha 1I$ subunits in a heterologous expression system display slow activation and inactivation kinetics that differ considerably from currents generated by $\alpha 1G$ and $\alpha 1H$ subunits (Chemin et al., 2002). The slow kinetics of $\alpha 1I$ -generated Ca^{2+} cur-

rents results in a significant entry of Ca^{2+} ions during an action potential. Transient currents generated by $\alpha 1\text{H}$ subunits are highly sensitive to blockade by low nickel concentrations (Lee et al., 1999). On the basis of our molecular characterization of a partial sequence of the $\alpha 1\text{H}$ subunit, we conclude that $\alpha 1\text{H}$ subunits mediate T-type Ca^{2+} currents in chick nodose neurons. We cannot, however, rule out the possibility that our set of primers will only recognize the chick $\alpha 1\text{H}$ subunit since none of the chick $\alpha 1$ isoforms have been sequenced. Nonetheless, three lines of evidence support our conclusion that $\alpha 1\text{H}$ subunits mediate most of T-type Ca^{2+} currents in chick nodose neurons. First, T-type Ca^{2+} currents in chick nodose neurons are highly sensitive to blockade by low concentrations of Ni^{2+} . Study of the concentration dependence of the Ni^{2+} blockade of T-type Ca^{2+} currents reveals an IC_{50} of $17 \mu\text{M}$, close to that previously reported for native channels in mouse embryonic vestibular ($\text{IC}_{50} = 13.4 \mu\text{M}$) and rat pelvic neurons ($\text{IC}_{50} = 10 \mu\text{M}$; Lee et al., 2002; Autret et al., 2005). This value is over 10-fold lower than the IC_{50} described for T-type Ca^{2+} currents generated by $\alpha 1\text{G}$ ($\text{IC}_{50} = 259 \mu\text{M}$) and $\alpha 1\text{I}$ subunits ($\text{IC}_{50} = 216 \mu\text{M}$, Lee et al., 1999). Second, analysis of deactivation tail currents supports the presence of only one population of T-type Ca^{2+} channels. Third, sequencing of our partial cDNA indicates a high level of similarity with the rat and human $\alpha 1\text{H}$ subunits, whereas the sequence similarity with $\alpha 1\text{G}$ and $\alpha 1\text{I}$ subunits from other species was somewhat lower. The possibility that $\alpha 1\text{H}$ subunits mediate T-type Ca^{2+} currents in chick nodose neurons is also compatible with previous findings in other species. For example, it has been reported that $\alpha 1\text{H}$ is the main subunit expressed in rat nodose neurons that form functional T-type Ca^{2+} channels (Lambert et al., 1998).

Characterization of the biophysical properties of T-type Ca^{2+} channels in chick nodose neurons is also consistent with Ca^{2+} currents generated by $\alpha 1\text{H}$ subunits. Activation and inactivation time constants are similar to those previously reported for Ca^{2+} currents generated by rat $\alpha 1\text{H}$ subunits in a heterologous expression system (Klockner et al., 1999). The values of steady-state activation and inactivation were also closely related to those generated by $\alpha 1\text{H}$ subunits in other mammalian neurons (Chemin et al., 2002; Lee et al., 2002; Autret et al., 2005). However, the deactivation time constant was significantly higher than previously reported in a heterologous expression system (Chemin et al., 2002). This may reflect the contribution of other factors to channel closure in native channels including the presence of other auxiliary

subunits and/or splice variants (Chemin et al., 2001; Green et al., 2001).

Similar to other T-type Ca^{2+} currents in developing neurons (McCobb et al., 1989; Gu and Spitzer, 1993; Martin-Caraballo and Greer, 2001), embryonic nodose neurons express Ca^{2+} currents with low threshold activation, rapid inactivation and high sensitivity to low concentrations of Ni^{2+} ions. However, differently from spinal cord neurons (McCobb et al., 1989; Gu and Spitzer, 1993; Martin-Caraballo and Greer, 2001), our present results reveal an incremental pattern of T-type Ca^{2+} channel functional expression in nodose neurons during embryonic development. Thus, T-type Ca^{2+} currents were present in a large population of nodose neurons between E17 and E20, whereas at earlier stages of development this current was restricted to a few neurons. Therefore, it appears that T-type Ca^{2+} channels undergo major changes in their functional expression at later stages of embryonic development. There are two important points that should be taken into consideration when interpreting the present results. First, it is unlikely that this pattern of T-type Ca^{2+} channel expression is due to the preferential loss of dendritic outgrowth during dissociation. According to previous findings, nodose neurons lack any significant dendritic component during the developmental stages used in our study (Harrison et al., 1994). We cannot, however, exclude the possibility that some differences in T-type Ca^{2+} channel distribution exist between various cellular compartments (such as soma, axon, or synaptic terminal) that cannot be assessed by our current recordings of somatic currents. Second, nodose neurons innervate different targets (heart, lungs, and other visceral tissues) with both mechanically and chemically activated nerve endings that send signals to the CNS (reviewed by Zhou et al., 1997). Therefore, it is possible that some differences may exist in the pattern of T-type Ca^{2+} channel expression based on target innervation and/or sensory information transmitted to the CNS.

Our current findings, taken together with previous studies (McCobb et al., 1989; Desmadryl et al., 1998; Schmid and Guenther, 1999; Martin-Caraballo and Greer, 2001), indicate that during neuronal differentiation two different patterns of T-type Ca^{2+} channel functional expression emerge in different neuronal populations. The first pattern is characterized by increased T-type Ca^{2+} channel expression and can be found in sensory neurons like nodose and dorsal root ganglia (Desmadryl et al., 1998). The second pattern has been identified in CNS neurons like hippocampal, retinal, and spinal neurons and is characterized by a significant reduction in T-type Ca^{2+} channel expres-

sion at early stages of embryonic development (McCobb et al., 1989; Chambard et al., 1999; Schmid and Guenther, 1999; Martin-Caraballo and Greer, 2001). Although our present results clearly indicate a significant increase in the functional expression of T-type Ca^{2+} channels in developing chick nodose neurons, our molecular data suggest that T-type Ca^{2+} channel transcripts are already present at E7. This surprising result would suggest that functional expression of T-type Ca^{2+} channels is regulated by a posttranscriptional mechanism. Although this is the first report indicating that functional expression of T-type Ca^{2+} channels is not coupled to the presence of channel transcripts, there is evidence that this may occur with other ion channels. For example, transcripts of large conductance, Ca^{2+} -dependent K^{+} channels are detected prior to their functional expression in chick ciliary neurons (Subramony et al., 1996). One attractive possibility is that extrinsic factors regulate the functional expression of T-type Ca^{2+} channels in developing chick nodose neurons. We have explored this possibility in the following article.

Differences in the expression pattern of T-type Ca^{2+} channels in sensory and spinal neurons indicate that they may play different functional roles during neuronal differentiation. Functionally, Ca^{2+} influx via T-type Ca^{2+} channels can regulate the development of membrane excitability as well as various Ca^{2+} -dependent developmental processes. For example, activation of T-type Ca^{2+} channels makes a significant contribution to the action potential waveform and the temporal pattern of repetitive firing in developing motoneurons (Umemiya and Berger, 1994; Martin-Caraballo and Greer, 2001). Indeed, our present results indicate that T-type Ca^{2+} channels are implicated in the generation of rebound depolarization, although they have very little effect on the action potential waveform. Activation of T-type Ca^{2+} channels following a hyperpolarizing input could potentially increase membrane excitability and activation of other voltage-dependent conductances (Gu and Spitzer, 1993; Martin-Caraballo and Greer, 2001). Similarly, Ca^{2+} influx through T-type Ca^{2+} channels regulates various developmental processes including maturation of axonal projections, dendritic outgrowth, and differentiation of electrical properties (Holliday and Spitzer, 1990; Gu and Spitzer, 1993).

We are grateful to Dr. Rae Nishi and Robert Schneider for helpful comments on the manuscript. We thank Dr. Sheryl White from the Center of Biomedical Research Excellence (COBRE) in Neuroscience at the University of Vermont for the design of the PCR primers used in this work. We are grateful to Thomas Trimarchi and Thomas

Buttolph for technical assistance with PCR analysis. The content of this work is solely the responsibility of the authors and does not necessarily represent the official views of NCRR or NIH.

REFERENCES

- Autret L, Mechaly I, Scamps F, Valmier J, Lory P, Desmadryl G. 2005. The involvement of Cav3.2/ α 1H T-type calcium channels in excitability of mouse embryonic primary vestibular neurones. *J Physiol* 567 (Part 1):67–78.
- Barish ME. 1991. Voltage-gated calcium currents in cultured embryonic *Xenopus* spinal neurones. *J Physiol* 444:523–543.
- Brosenitsch TA, Salgado-Commissariat D, Kunze DL, Katz DM. 1998. A role for L-type calcium channels in developmental regulation of transmitter phenotype in primary sensory neurons. *J Neurosci* 18:1047–1055.
- Catterall WA. 1998. Structure and function of neuronal Ca^{2+} channels and their role in neurotransmitter release. *Cell Calcium* 24:307–323.
- Chambard JM, Chabbert C, Sans A, Desmadryl G. 1999. Developmental changes in low and high voltage-activated calcium currents in acutely isolated mouse vestibular neurons. *J Physiol* 518 (Part 1):141–149.
- Chemin J, Monteil A, Bourinet E, Nargeot J, Lory P. 2001. Alternatively spliced α (1G) (Ca(V)3.1) intracellular loops promote specific T-type Ca^{2+} channel gating properties. *Biophys J* 80:1238–1250.
- Chemin J, Nargeot J, Lory P. 2002. Neuronal T-type α 1H calcium channels induce neurogenesis and expression of high-voltage-activated calcium channels in the NG108-15 cell line. *J Neurosci* 22:6856–6862.
- Cribbs LL, Lee JH, Yang J, Satin J, Zhang Y, Daud A, Barclay J, et al. 1998. Cloning and characterization of α 1H from human heart, a member of the T-type Ca^{2+} channel gene family. *Circ Res* 83:103–109.
- D'Amico-Martel A. 1982. Temporal patterns of neurogenesis in avian cranial sensory and autonomic ganglia. *Am J Anat* 163:351–372.
- Desmadryl G, Hilaire C, Vignes S, Diochot S, Valmier J. 1998. Developmental regulation of T-, N- and L-type calcium currents in mouse embryonic sensory neurones. *Eur J Neurosci* 10:545–552.
- Forgie A, Doxakis E, Buj-Bello A, Wyatt S, Davies AM. 1999. Differences and developmental changes in the responsiveness of PNS neurons to GDNF and neurturin. *Mol Cell Neurosci* 13:430–440.
- Fox AP, Nowycky MC, Tsien RW. 1987. Single-channel recordings of three types of calcium channels in chick sensory neurons. *J Physiol* 394:173–200.
- Green PJ, Warre R, Hayes PD, McNaughton NC, Medhurst AD, Pangalos M, Duckworth DM, et al. 2001. Kinetic modification of the α (II) subunit-mediated T-type Ca^{2+} channel by a human neuronal Ca^{2+} channel γ subunit. *J Physiol* 533 (Part 2):467–478.
- Gottmann K, Dietzel ID, Lux HD, Huck S, Rohrer H. 1988. Development of inward currents in chick sensory and au-

- tonomic neuronal precursor cells in culture. *J Neurosci* 8:3722–3732.
- Gu X, Spitzer NC. 1993. Low-threshold Ca^{2+} current and its role in spontaneous elevations of intracellular Ca^{2+} in developing *Xenopus* neurons. *J Neurosci* 13:4936–4948.
- Harrison TA, Stadt HA, Kirby ML. 1994. Developmental characteristics of the chick nodose ganglion. *Dev Neurosci* 16:67–73.
- Harrison TA, Stadt HA, Kumiski D, Kirby ML. 1995. Compensatory responses and development of the nodose ganglion following ablation of placodal precursors in the embryonic chick (*Gallus domesticus*). *Cell Tissue Res* 281:379–385.
- Holliday J, Spitzer NC. 1990. Spontaneous calcium influx and its roles in differentiation of spinal neurons in culture. *Dev Biol* 141:13–23.
- Iwasaki S, Momiyama A, Uchitel OD, Takahashi T. 2000. Developmental changes in calcium channel types mediating central synaptic transmission. *J Neurosci* 20:59–65.
- Klockner U, Lee JH, Cribbs LL, Daud A, Hescheler J, Pereverzev A, Perez-Reyes E, et al. 1999. Comparison of the Ca^{2+} currents induced by expression of three cloned $\alpha 1$ subunits, $\alpha 1G$, $\alpha 1H$ and $\alpha 1I$, of low-voltage-activated T-type Ca^{2+} channels. *Eur J Neurosci* 11:4171–4178.
- Lambert RC, McKenna F, Maulet Y, Talley EM, Bayliss DA, Cribbs LL, Lee JH, et al. 1998. Low-voltage-activated Ca^{2+} currents are generated by members of the CavT subunit family ($\alpha 1G/H$) in rat primary sensory neurons. *J Neurosci* 18:8605–8613.
- Larmet Y, Dolphin AC, Davies AM. 1992. Intracellular calcium regulates the survival of early sensory neurons before they become dependent on neurotrophic factors. *Neuron* 9:563–574.
- Lee JH, Gomora JC, Cribbs LL, Perez-Reyes E. 1999. Nickel block of three cloned T-type calcium channels: Low concentrations selectively block $\alpha 1H$. *Biophys J* 77:3034–3042.
- Lee JH, Kim EG, Park BG, Kim KH, Cha SK, Kong ID, Lee JW, et al. 2002. Identification of T-type $\alpha 1H$ Ca^{2+} channels (Ca(v)3.2) in major pelvic ganglion neurons. *J Neurophysiol* 87:2844–2850.
- Lindsay RM, Thoenen H, Barde YA. 1985. Placode and neural crest-derived sensory neurons are responsive at early developmental stages to brain-derived neurotrophic factor. *Dev Biol* 112:319–328.
- Martin-Caraballo M, Dryer SE. 2002. Activity- and target-dependent regulation of large-conductance Ca^{2+} -activated K^{+} channels in developing chick lumbar motoneurons. *J Neurosci* 22:73–81.
- Martin-Caraballo M, Greer JJ. 2001. Voltage-sensitive calcium currents and their role in regulating phrenic motoneuron electrical excitability during the perinatal period. *J Neurobiol* 46:231–248.
- McCobb DP, Best PM, Beam KG. 1989. Development alters the expression of calcium currents in chick limb motoneurons. *Neuron* 2:1633–1643.
- McRory JE, Santi CM, Hamming KS, Mezeyova J, Sutton KG, Baillie DL, Stea A, et al. 2001. Molecular and functional characterization of a family of rat brain T-type calcium channels. *J Biol Chem* 276:3999–4011.
- Mittman S, Guo J, Agnew WS. 1999. Structure and alternative splicing of the gene encoding $\alpha 1G$, a human brain T calcium channel $\alpha 1$ subunit. *Neurosci Lett* 274:143–146.
- Mulroy MJ, Harrison TA. 1994. Developmental study of the long QT with deafness syndrome in the chick embryo: Cochlear pathology. *Int J Pediatr Otorhinolaryngol* 29:179–194.
- Murbartian J, Arias JM, Lee JH, Gomora JC, Perez-Reyes E. 2002. Alternative splicing of the rat Ca(v)3.3 T-type calcium channel gene produces variants with distinct functional properties. *FEBS Lett* 528:272–278.
- Perez-Reyes E, Cribbs LL, Daud A, Lacerda AE, Barclay J, Williamson MP, Fox M, et al. 1998. Molecular characterization of a neuronal low-voltage-activated T-type calcium channel. *Nature* 391:896–900.
- Schmid S, Guenther E. 1999. Voltage-activated calcium currents in rat retinal ganglion cells in situ: Changes during prenatal and postnatal development. *J Neurosci* 19:3486–3494.
- Subramony P, Raucher S, Dryer L, Dryer SE. 1996. Post-translational regulation of Ca^{2+} -activated K^{+} currents by a target-derived factor in developing parasympathetic neurons. *Neuron* 17:115–124.
- Umemiya M, Berger AJ. 1994. Properties and function of low- and high-voltage-activated Ca^{2+} channels in hypoglossal motoneurons. *J Neurosci* 14:5652–5660.
- Vogel KS, Davies AM. 1991. The duration of neurotrophic factor independence in early sensory neurons is matched to the time course of target field innervation. *Neuron* 7:819–830.
- Zhuo H, Ichikawa H, Helke CJ. 1997. Neurochemistry of the nodose ganglion. *Prog Neurobiol* 52:79–107.